Warping Effect-Induced Spin Current Absorption at Various Timescales in Fe/Bi_2Te_3 Heterostructures

Jia-nan Liu,[1,2] Hao-Pu Xue,[1,2] Zhuo Deng,[1,2] Qing-Lin Yang,[1,2] Xiao-Min Li,[1] Xue-Dong Bai,[1,2,3] Xu Yang,[1,2,3] Peng-Tao Yang,[1,2] Yu-Han Gao,[1,2] Wei He,[1] Xiang-Qun Zhang,[1] and Zhao-Hua Cheng[1,2,3,*]

[1]*Beijing National Laboratory for Condensed Matter Physics, Institute of Physics, Chinese Academy of Sciences, Beijing 100190, China*
[2]*School of Physical Sciences, University of Chinese Academy of Sciences, Beijing 100049, China*
[3]*Songshan Lake Materials Laboratory, Dongguan, Guangdong 523808, China*

(Received 16 August 2024; accepted 5 May 2025; published 13 June 2025)

The spin pumping in ferromagnet/nonmagnetic materials (FM/NM) heterostructures is an effective technique to inject spin current into NM, which provides the possibility of ultrafast, low-power consumption spintronic devices. Previous work demonstrates that the high order terms in $\mathbf{k} \cdot \mathbf{p}$ theory can induce a large warping effect, and consequently snowflakelike Fermi contour in topological insulator (TI). Unfortunately, the effect of warped topological surface state (TSS) on pure spin absorption in FM/TI heterostructures is completely unknown. Here, by considering strength of spin accumulation, we identified a mechanism for the anisotropic absorption of spin current in a FM/TI heterostructure with a large warping effect. If the density of states (DOS) of TSS dominates at the Fermi surface, the warping effect results in an anisotropic Gilbert damping at nanosecond timescale and almost isotropic ultrafast demagnetization time at femtosecond timescale. The anisotropy of Gilbert damping is found to decrease as bulk state contributions become more significant in thicker Bi_2Te_3 films. Our theoretical predictions regarding the warping effect-induced spin current absorption at nanosecond and subpicosecond timescales have been experimentally validated in Fe/Bi_2Te_3 heterostructures by ferromagnetic resonance and time-resolved magneto-optical Kerr effect (TRMOKE) results, respectively. Our work provides a more intuitional way to understand the spin transfer mechanism, and lays the groundwork for advancing anisotropic spintronics.

DOI: 10.1103/PhysRevLett.134.236204

Introduction—The dynamics of magnetization in ferromagnetic materials (FM) can transfer spin angular momentum into the nonmagnetic materials (NM) in their heterostructures. At the nanosecond timescale, the spin pumping effect is a widely utilized approach for generating spin potential in NM and enhancing Gilbert damping of FM/NM heterostructures [1–4]. At the femtosecond timescale, spin angular momentum is carried by excited electrons and injected into NM in the form of superdiffusion [5–7]. Combined with the different types of NM with strong spin-orbit coupling (SOC), these processes enable various applications, such as spin-charge conversion [8,9], spintronics [10,11], and terahertz (THz) wave manipulation [12,13]. Recently, we found an anisotropic spin-mixing conductance (SMC) in FM/GeTe [14], which offers new opportunities for anisotropic spin-transfer torque-based devices. However, the bulk Rashba effect of GeTe arises from inversion symmetry breaking, which disappears when the GeTe thickness is reduced to below ~10 nm. Furthermore, the SMC depends solely on the interfacial properties of the heterostructure, making it challenging to analyze. Therefore, the anisotropic absorption of spin current could serve as an ideal mechanism for advancing anisotropic spintronics.

The topological surface state (TSS) in $\mathbb{Z}_2$ topological insulators (TIs) has a variety of Fermi contour forms with spin-momentum locking [15–17]. As shown in Fig. 1(a), different from the ideally circular shape of Fermi contours in the Dirac materials, Bi_2Te_3 has a snowflakelike Fermi surface as well as an anisotropic spin lifetime, which is related to the so-called warping effect [18,19]. Previous theories have predicted that this distortion of the Dirac cone might induce some interesting phenomena, such as the enhanced surface scattering [18,19] and the surface spin-density waves [19]. The bilinear magnetoelectric resistance has also been confirmed experimentally by the warping effect [20]. One can expect that warped TSS would induce an anisotropic absorption of spin current, leading to an anisotropic enhanced Gilbert damping in FM/TI heterostructures. Since the spin pumping and the spin transfer are two fundamentally equivalent dynamis according to Onsager's reciprocity relations [21,22], it is reasonable to expect that the enhanced Gilbert damping can facilitate the SOT switching. This would underscore the promising application potential of TIs in devices with low switching current density and power dissipation [23,24]. In this work, we build up a toy model to investigate the impact of the warping effect of TSS on spin

*Contact author: zhcheng@iphy.ac.cn

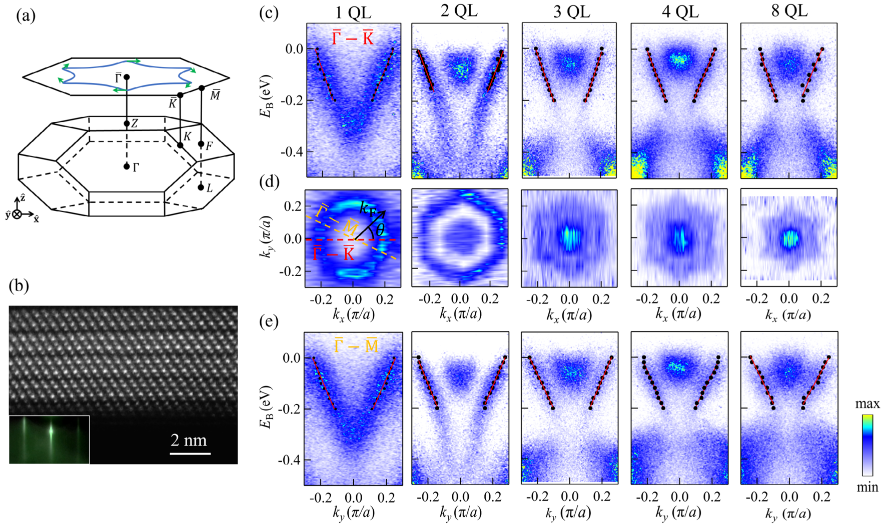

FIG. 1. Warping effect of Bi_2Te_3 with different thicknesses. (a) The 3D Brillouin zoom and its projected onto the 2D Brillouin zone along c axis of Bi_2Te_3 with the high symmetrical points. The blue curve represents a typical Fermi contour of the TSS, with the spin texture labeled by green arrows. (b) HAADF image of Bi_2Te_3. The inset shows the RHEED pattern of Bi_2Te_3. (c)–(e) ARPES spectra along $\bar{\Gamma}-\bar{\mathrm{K}}$, Fermi surfaces, and $\bar{\Gamma}-\bar{\mathrm{M}}$, respectively. The corresponding thicknesses are labeled at the top of each column. The black dots indicate fitted peak position by Lorentzian function of MDCs, and the red lines represent linear fitting results of black dots. The red and orange dotted line in the Fermi surface of the 1 QL sample labels the direction of $\bar{\Gamma}-\bar{\mathrm{K}}$ and $\bar{\Gamma}-\bar{\mathrm{M}}$. The black arrow indicates the Fermi wave vector $k_{\mathrm{F}}(\theta)$.

pumping in FM/TI heterostructure. Our model shows that the distribution of spin accumulation on the Fermi contour of TSS can be dramatically influenced by the inter-band scattering, and an anisotropic Gilbert damping induced by the spin pumping effect is evident when the high-quality Bi_2Te_3 layer is very thin. Experimentally, we investigated the warping effect of ultrathin Bi_2Te_3 film and the Gilbert damping in Fe/Bi_2Te_3 heterostructures via angle-resolved photoemission spectroscopy (ARPES) and ferromagnetic resonance (FMR), respectively. We find that a sixfold anisotropic Gilbert damping exists in this system and the anisotropic damping ratio diminishes with increasing the thickness of Bi_2Te_3 as the contribution of bulk state increases. This behavior of anisotropic Gilbert damping is different from the case of Fe/GaAs [25] and FM/GeTe [14], but similar to the case of $Co_{50}Fe_{50}/Cr/Ni_{81}Fe_{19}$ spin valve [26], which is attributed to anisotropic absorption of spin current. Furthermore, the ultrafast demagnetization process is also investigated by the toy model theoretically and the time-resolved magneto-optical Kerr effect (TRMOKE) experimentally. As expected, the anisotropy of ultrafast demagnetization time is suppressed since the steady state of spin accumulation has not yet been reached within the femtosecond timescale. Our research presents a novel mechanism for spin current absorption across different timescales, offering new insights into the dynamics of spin currents in FM/TI heterostructures.

Theory—Similar to the cases in most heterostructures [27,28], we can express the Hamiltonian of a FM/TI heterostructure as

$$\mathcal{H} = \mathcal{H}_{\mathrm{FM}}\Theta(z) + \mathcal{H}_{\mathrm{TI}}\Theta(-z) + V_{\mathrm{surf}}(z) + V_{\mathrm{imp}}(\mathbf{r}), \qquad (1)$$

where $\mathcal{H}_{\mathrm{FM}}$ and $\mathcal{H}_{\mathrm{TI}}$ are the effective Hamiltonians of FM and TI layers, respectively. V_{surf} is the potential at the interface, V_{imp} describes the effect of impurities, and $\Theta(z)$ is the step function that defines the spatial separation between the layers. In the case of TI layer, both TSS and bulk states can contribute to the spin pumping effect. According to the low-energy effective model, the electrons in bulk states in typical $\mathbb{Z}_2$ TIs with a parabolic dispersion relation near the Γ point, such as Bi_2Se_3, Bi_2Te_3, and Sb_2Te_3 [15], can be treated as massive Dirac fermions. Therefore, we model the bulk state as a typical heavy metal. Assuming that the in-plane transitional symmetry is conserved at the interface, the transmission rate between a $\mathbf{m}$-polarized FM $|\Psi_{\boldsymbol{\kappa},\mathbf{m}}\rangle$ and the TSS $|\Phi_{\mathbf{s}}\rangle$ is $P(\mathbf{m};\mathbf{s}) = \frac{1}{2}P_0(1+\mathbf{s}\cdot\mathbf{m})$ [29], where $P_0 = \sum_{\kappa_z}|\int \mathrm{d}z\psi^*_{\kappa_z}(z)V_{\mathrm{surf}}(z)\phi(z)|^2$, $\psi_{\kappa_z}(z)$ and $\phi(z)$ are the z component of $\Psi_{\boldsymbol{\kappa},\mathbf{m}}(\mathbf{r})$ and $\Phi_{\mathbf{s}}(\mathbf{r})$, respectively. It should be noted that when the FM layer is sufficiently thick, the summation of κ_z will make P_0 quite large. Thus, it is reasonable to assume that $P_0 \gg 1$ in this work. The Boltzmann equation describing the non-equilibrium spin accumulation of TSS $n(\theta)$ at Fermi energy is

$$\partial_t n(\theta) = P(\mathbf{m}, \mathbf{s}_{\mathrm{F}}(\theta))(\mu_{\mathrm{s}} - n(\theta)) - \Gamma_{\mathrm{out}}(\theta) + \Gamma_{\mathrm{in}}(\theta), \qquad (2)$$

where μ_{s} is the spin potential caused by the spin pumping effect, $\Gamma_{\mathrm{in(out)}}$ is the rate at which electrons are scattered into (out of) the TSS $|\Phi_{\mathbf{s}(\theta)}\rangle$, and $\mathbf{s}_{\mathrm{F}}(\theta)$ is the spin texture of TSS near Fermi energy, and $\theta = \arctan(k_y/k_x)$. The scattering rate of TSS τ_F^{-1} is divided into the intraband scattering rate of TSS, τ_S^{-1}, and the interband scattering one between TSS and TI bulk state, τ_B^{-1}, i.e., $\tau_F^{-1} = \tau_S^{-1} + \tau_B^{-1}$. Here, we analyze three cases via introducing a dimensionless parameter $\eta(\theta) \equiv 8\pi P_0^{-1}\tau_F^{-1}(\theta)$ to describe the strength of spin accumulation in the TSS.

Case I: For the relatively thick TI layer with strong intra- and interband scattering, i.e., large $\tau_F^{-1}(\theta)$ and, consequently, $\eta(\theta) \gg 1$. In this case, the $\tau_F^{-1}(\theta) \gg P_0$ and the short spin relaxation time makes spin accumulation weak. One can obtain that

$$n(\theta) \approx \frac{\mu_s}{2\eta(\theta)}\mathbf{m}\cdot\mathbf{s}_F(\theta) + \text{const}, \tag{3}$$

Consequently, the spin current I_s remains unaffected by the direction of $\mathbf{m}$, resulting in an isotropic pumped spin current.

Case II: For the relatively thin TI layer, τ_F^{-1} can be small, and $\eta(\theta) \ll 1$. In this case, the $\tau_F^{-1}(\theta) \ll P_0$, and the long spin relaxation time results in a strong spin accumulation. With linear approximation, we can calculate the total spin current pumping into the TI layer as

$$I_{\text{tot}} = \mu_s\left[P_B N_{F,B}\left(\frac{1}{2}M_0 N_{F,S} + 1\right) + \frac{k_F(\theta_0)}{v_F(\theta_0)}\mathcal{S}(\theta_0)\right], \tag{4}$$

where the first and second terms in the square bracket correspond to the isotropic and anisotropic parts of I_{tot}, respectively. $N_{F,B}$ and $N_{F,S}$ are the density of states (DOS) of bulk states and TSS at Fermi energy, respectively. M_0 is the averaged scattering cross-section of interband scattering. $\mathcal{S}(\theta) = \sqrt{\eta(\theta)}((P_B + 2)\tau_B^{-1} + \{6 - [\tau_B^{-1}/\tau_F^{-1}(\theta)]P_B\}\tau_S^{-1}(\theta))$, and θ_0 is defined by $\mathbf{s}_F(\theta_0) = -\mathbf{m}$. Since the enhanced Gilbert damping is proportional to the pumped spin current $\alpha_{sp} \propto I_{\text{tot}}$, an anisotropic enhanced Gilbert damping can be predicted if two conditions are met: (i) the DOS of TSS dominates at the Fermi surface ($\eta \ll 1$), and (ii) the warping effect is significant (k_F/v_F is anisotropic). We anticipate that the high-quality ultrathin TI film with an anisotropic Fermi contour can satisfy these conditions.

Case III: The thickness of the TI layer is intermediate between case I and case II, and the η is not sufficiently small. By treating the bulk states as the electrons in a square box well, and taking the band shifting of TSS into account [30], we found the TI thickness depdence of average and part of enhanced Gilbert damping, $\overline{\alpha_{sp}}$ and $(\alpha_{\max} - \alpha_{\min})$ can be expressed as follow

$$\alpha_{\max} - \alpha_{\min} \propto \exp\left[-12\sqrt{t/\lambda_a + \beta_a}\right], \tag{5}$$

$$\overline{\alpha_{sp}} \propto t\left(e^{-t/\lambda} + \beta_0\right), \tag{6}$$

where t is the thickness of TI layer, $\lambda_a = t/P_0^{-1}M_0 N_{F,B}$, λ is the screening length of TSS, which is approximately equal to 1 nm for Bi_2Te_3 [31], $\beta_a = 8\pi P_0^{-1}\tau_S^{-1}$, and $\beta_0 = (2M_0^{-1} + N_{F,S,0})/\Delta N_{F,S}$, with the relation of $N_{F,S}$ and the TI thickness $N_{F,S} = N_{F,S,0} + \Delta N_{F,S}e^{-t/\lambda}$ [30]. Above all, we predicted that, with increasing thickness of TI layer, the anisotropic enhanced damping induced by warping effect will decrease exponentially, while the average part of enhanced damping will show a nonmonotonic behavior. The detailed description can be found in Supplemental Material S.IV [32].

Results—The ultrathin film is an ideal system because the large surface-bulk ratio restrains the effect of bulk states. Combined with the theory of band shifting in ultrathin TI films [30], the Fermi energy and DOS at the Fermi surface can be manipulated by changing the thickness. Figure 1(a) represents the 3D Brillouin zone of Bi_2Te_3. On the projected 2D Brillouin zone along the k_z axis, a typical Fermi contour of TSS is labeled by the blue curve, with its spin texture labeled by the green arrows. In this work, we choose the coordinate with $\hat{\mathbf{x}}\|\bar{\Gamma} - \bar{\mathrm{K}}$ and $\hat{\mathbf{y}}\|\bar{\Gamma} - \bar{\mathrm{M}}$. Here, we first analyzed the Fermi contour of TSS in Bi_2Te_3/Si (111) with different thicknesses of Bi_2Te_3 layers by ARPES. We use the standard molecular beam epitaxy (MBE) technique to grow Bi_2Te_3 [t quintuple layers (QL)]/Si(111) with $t = 1$, 2, 3, 4, and 8 QL (1 QL ≈ 0.9 nm). Figure 1(b) shows the morphology of Bi_2Te_3 by high-angle annular dark-field (HAADF) image with its reflection high-energy electron diffraction (RHEED) pattern. The ARPES spectra of these samples are shown in Figs. 1(c)–1(e). The Fermi surface shows a significant warping effect in all samples except for 1 QL film. The magnetic dynamics at the nanosecond timescale was investigated by the vector network analyzer (VNA) FMR with prepared Fe (8 nm)/Bi_2Te_3 (t)/Al_2O_3 (0001) samples, as shown in Fig. 2(a). During sample preparation, we found that the Fe layer is epitaxially grown on the Bi_2Te_3 layer, as confirmed by RHEED patterns shown in Fig. S1 [32], making the expression of $P(\mathbf{s}, \mathbf{m})$ holds.

Here, we define φ as the angle between external field $\mathbf{H}$ and $\bar{\Gamma} - \bar{\mathrm{K}}$, i.e., $\varphi \equiv \langle \mathbf{H}, \bar{\Gamma} - \bar{\mathrm{K}}\rangle = \langle \mathbf{H}, \hat{\mathbf{x}}\rangle$. According to our theory, when $\mathbf{H}\|\bar{\Gamma} - \bar{\mathrm{M}}$ and $\eta \ll 1$, the spin-momentum locked Dirac fermion makes $\theta_0 \approx \varphi - 90°$ in Eq. (4). The coresponding n and I_{tot} are shown in Figs. 2(b) and 2(c), respectively. The latter causes an enhanced Gilbert damping, which can be extracted by linearly fitting the full-width at half maximum (FWHM) ΔH of Lorentzian peaks versus frequency f. More details of the FMR analysis are provided in the Supplemental Material [32]. The φ-dependent enhanced Gilbert damping by spin pumping $\alpha_{sp}(\varphi) = \alpha(\varphi) - \alpha_{Fe}$ in the samples of $t = 1, 2, 3, 4$, and 8 QL are shown in Figs. 2(d)–2(h), where the Gilbert damping of Fe is $\alpha_{Fe} \approx 0.004$ [25]. First, we extracted both

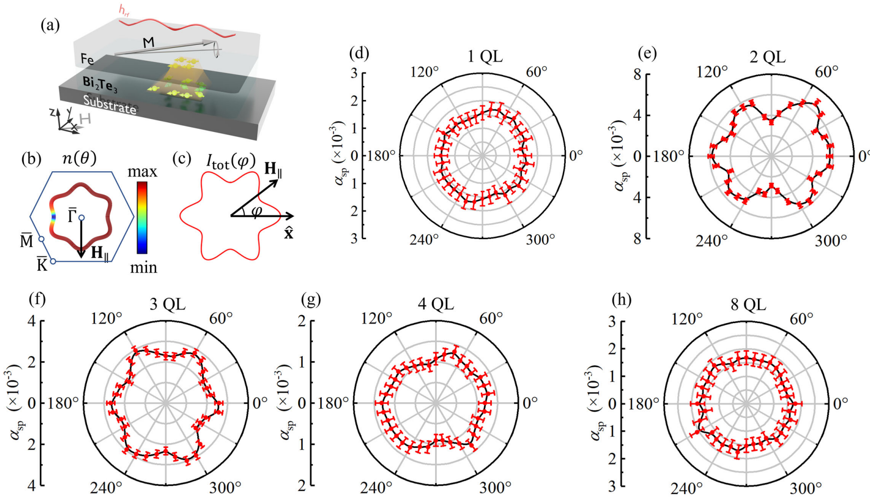

FIG. 2. Anisotropic Gilbert damping in Fe/Bi_2Te_3. (a) Schematic illustration of the measurement configuration of FMR in Fe/Bi_2Te_3. (b) Sketch of the accumulation of spin $n(\theta)$ on Fermi contour when the in-plane part of the magnetic field orientate to the $-\hat{\mathbf{y}}$ direction. (c) The external field orientation related injected spin current after integrating the density. (d)–(h) Magnetic field orientation φ dependent enhanced Gilbert damping in Fe (8 nm)/Bi_2Te_3 (t QL)/Al_2O_3 samples with $t = 1$, 2, 3, 4, and 8 QL.

the anisotropic damping ratio $\{[\max(\alpha_{sp}) - \min(\alpha_{sp})]/\min(\alpha_{sp})\} \times 100\%$ and the average value $\overline{\alpha_{sp}} \equiv \overline{\alpha_{sp}(\varphi)}$, as shown in Figs. 3(a) and 3(b), respectively. The nonmonotonic behavior of $\overline{\alpha_{sp}}$ appears as expected, and is very similar to the case in Bi_2Se_3/YIG [39]. The mechanism of dilution by bulk state is also very similar to the case in spin-orbital torque (SOT) efficiency [24]. Since the screening length of Bi_2Te_3 is $\lambda \approx 1$ nm, which is much thinner than Bi_2Se_3 of ~ 3 nm [30,31], the thickness corresponding to the maximum of $\overline{\alpha}$ is also found smaller than that in Bi_2Se_3. The anisotropic damping ratio also decreases with increasing TI thickness, and such behavior is different from all reported anisotropic damping in heterojunctions, as far as we know [14,25,40]. Then, we fitted the position of energy band, labeled by black dots in Figs. 1(c) and 1(e), and extracted v_F and k_F. The v_F/k_F versus thickness in the directions of $\bar{\Gamma} - \bar{M}$ and $\bar{\Gamma} - \bar{K}$ is shown in Fig. 3(c). The details of the fitting procedure are available in S.III [32]. Since no warping effect was observed in Bi_2Te_3 (1 QL), the φ-dependent enhanced Gilbert damping $\alpha_{sp}(\varphi)$ of Fe/Bi_2Te_3 (1 QL) indicates nearly isotropic behavior. With increasing t, the sixfold symmetric anisotropy of the enhanced damping becomes evident owing to the enhancement of the warping effect. However, for the relatively thick samples, intra- and interband scattering are strong, i.e., large $\tau_F^{-1}(\theta)$ and, consequently, $\eta(\theta) \gg 1$. Consequently, I_s remains unaffected by the direction of $\mathbf{m}$, resulting in an isotropic spin current. Therefore, although the Fermi surface exhibits more pronounced warping, the anisotropy of enhanced damping diminishes with further increasing t.

As discussed in case III and Supplemental Material [32], the fiting results of $\overline{\alpha_{sp}}$ and $(\alpha_{max} - \alpha_{min})$ versus $N_{F,S}$ with Eqs. (5) and (6) are shown by red lines in Figs. 3(a) and 3(b), respectively. For Bi_2Te_3, the screening length $\lambda = 1$ nm is used by previous ARPES study [31]. The fitting results shows that $8\pi P_0^{-1}\tau_S^{-1} \approx 2.5 \times 10^{-3}$, and $8\pi P_0^{-1}\tau_B^{-1}/t \approx 0.017$ nm^{-1}. The discrepancy between the enhanced damping in 1 QL and the fitted result primarily originates from the near disappearance of the warping effect in 1 QL Bi_2Te_3. This phenomenon eliminates anisotropy and significantly reduces $N_{F,S}$. Above all, we

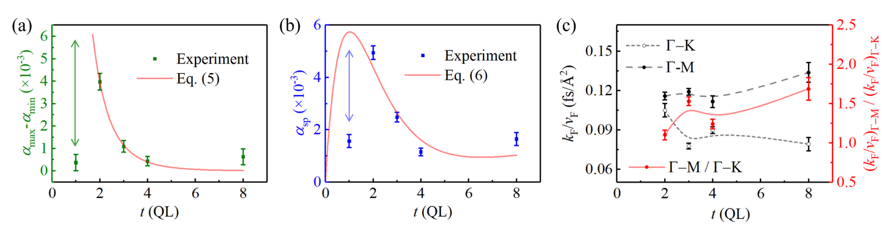

FIG. 3. The relationship between anisotropic Gilbert damping and TSS. (a) and (b) The anisotropic (green) and average (blue) parts of Gilbert damping as a function of TI layers thickness with red fitting lines derived from Eqs. (5) and (6), respectively. The double-side arrow shows the difference between theoretical results [Eqs. (5) and (6)] and the experimental data for the sample with $t = 1$ QL. (c) The relationship between k_F/v_F and thickness in different directions (black dotted lines), and their ratio (red line).

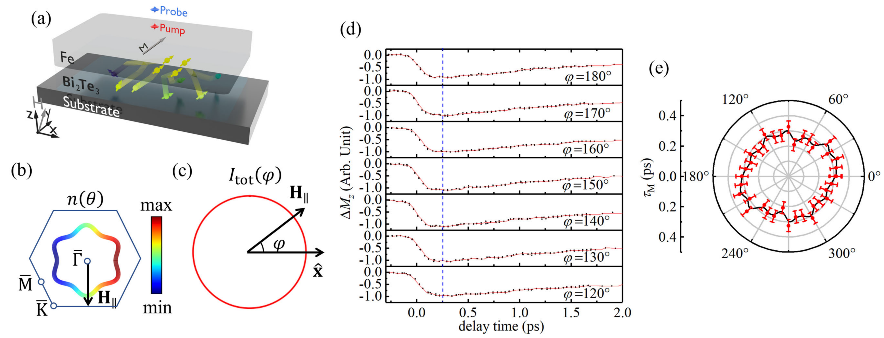

FIG. 4. TRMOKE measurements of Fe (8 nm)/Bi_2Te_3(3 QL)/Al_2O_3. (a) Schematic illustration of measurement configuration of TRMOKE. (b) Sketch of a typical $n(\theta)$ by Eq. (3). (c) The external field orientation related spin current after integrating the density. (d) Ultrafast demagnetization curves for different in-plane magnetic field directions, with the fitted demagnetization time represents in (e). The blue dashed line serves as a guide for the eye.

find that the warping effect alone is insufficient to account for anisotropic Gilbert damping. Additionally, the DOS of TSS must dominate at the Fermi surface. Previous work has demonstrated that as the thickness of Bi_2Te_3 films increases, the Fermi energy shifts towards the Dirac point, resulting in the reduction of the DOS of TSS [31]. Meanwhile, the DOS of bulk states significantly increases and reaches saturation with increasing film thickness. Consequently, the nontrivial distribution illustrated in Fig. 2(b) is no longer established, resulting in isotropy.

Understanding the spin dynamics from nanosecond to femtosecond timescales is crucial for the realization of ultrafast spintronic devices in the frequency range from gigahertz to terahertz [41,42]. During ultrafast demagnetization, ultrafast spin current plays a key role in transferring the angular momentum, which can generate THz waves through spin-charge conversion in the NM layer [43,44]. Although no anisotropy in normalized THz efficiency was observed and analyzed by the inverse Rashba-Edelstein effect tensor, it remains unclear whether the spin injection itself exhibits anisotropy [43,44]. The TRMOKE technique can provide an effective means to probe the ultrafast demagnetization time τ_M, and investigate the effect of the strong spin accumulation at warped TSS on the anisotropy of spin injection of Fe/Bi_2Te_3. Therefore, we further measured the ultrafast demagnetization of Fe (8 nm)/Bi_2Te_3(3 QL)/Al_2O_3 by TRMOKE technique, with the experimental setup presented in Fig. 4(a). After being pumped by the laser pulse, the excited spin-polarized electrons exhibit superdiffusive motion over several hundreds of femtoseconds [5,6,45]. In this ultrashort period, the superdiffusive time of laser-induced spin current is comparable with the electron scatting one, preventing the establishment of a steady state of spin accumulation. Since the electron can only move $\sim 10^1$ nm in the in-plane direction, and even shorter in the out-of-plane direction, we simplify our analysis by neglecting the complicated interfacial reflection associated with superdiffusion [45]. The rate of spin injection into the TSS $|\Phi_{\mathbf{k}(\mathbf{s})}\rangle$ should be equivalent to $P(\mathbf{m},\mathbf{s})$, and a typical nonequilibrium spin distribution on a constant energy contour is shown in Fig. 4(b). $P(\mathbf{m},\mathbf{s})$ has a simply linear form of $\mathbf{s}$. Therefore, the ultrafast demagnetization time τ_M is defined by the dynamic equation of the density of excited electron in FM n_{FM}

$$\partial_t n_{FM} = -n_{FM}\int \mathrm{d}\mathbf{s}\, P(\mathbf{m},\mathbf{s}) \equiv -\frac{n_{FM}}{\tau_M} \tag{7}$$

should be isotropic after the intergral over $\mathbf{s}$. The ultrafast demagnetization curves with different magnetic field directions are shown in Fig. 4(d). The ultrafast demagnetization time τ_M is extracted by identifying the maximum of demagnetization [46,47], and the φ-dependent τ_M is presented in Fig. 4(e). Notably, unlike the FMR case, the sixfold anisotropic ultrafast spin dynamics is not evident at subpicosecond timescale.

Conclusion—In summary, based on the significant difference in the spatial distribution of the wave function between TSS and bulk state in heavy metals, we proposed a mechanism for the anisotropic absorption of spin current in a FM/TI heterostructure with a large warping effect. We predict that this warping effect leads to an anisotropic enhancement of Gilbert damping at the nanosecond timescale and nearly isotropic ultrafast demagnetization time at the femtosecond timescale. Our theoretical predictions have been experimentally verified in Fe/Bi_2Te_3 heterostructures by FMR and TRMOKE techniques. Our work provides an intuitive understanding of spin transferring in heterostructures and an additional degree of freedom to manipulate the spintronic devices across various timescales.

Acknowledgments—This work was supported by the National Key R&D Program of China (Grant No. 2022YFA1403302) and the National Natural Sciences Foundation of China (Grants No. U22A20115 and No. 52031015).

[1] Y. Tserkovnyak, A. Brataas, and G. E. W. Bauer, Enhanced Gilbert damping in thin ferromagnetic films, Phys. Rev. Lett. **88**, 117601 (2002).

[2] Y. Tserkovnyak, A. Brataas, and G. E. W. Bauer, Spin pumping and magnetization dynamics in metallic multilayers, Phys. Rev. B **66**, 224403 (2002).

[3] A. Brataas, Y. V. Nazarov, and G. E. W. Bauer, Finite-element theory of transport in ferromagnet–normal metal systems, Phys. Rev. Lett. **84**, 2481 (2000).

[4] Y. Tserkovnyak, A. Brataas, G. Bauer, and B. Halperin, Nonlocal magnetization dynamics in ferromagnetic heterostructures, Rev. Mod. Phys. **77**, 1375 (2004).

[5] M. Battiato, K. Carva, and P. M. Oppeneer, Superdiffusive spin transport as a mechanism of ultrafast demagnetization, Phys. Rev. Lett. **105**, 027203 (2010).

[6] M. Battiato, K. Carva, and P. M. Oppeneer, Theory of laser-induced ultrafast superdiffusive spin transport in layered heterostructures, Phys. Rev. B **86**, 024404 (2012).

[7] D. Rudolf *et al.*, Ultrafast magnetization enhancement in metallic multilayers driven by superdiffusive spin current, Nat. Commun. **3**, 1037 (2012).

[8] V. M. Edelstein, Spin polarization of conduction electrons induced by electric current in two-dimensional asymmetric electron systems, Solid State Commun. **73**, 233 (1990).

[9] W. Han, Y. Otani, and S. Maekawa, Quantum materials for spin and charge conversion, npj Quantum Mater. **3**, 27 (2018).

[10] S. A. Wolf, D. D. Awschalom, R. A. Buhrman, J. M. Daughton, S. von Molnár, M. L. Roukes, A. Y. Chtchelkanova, and D. M. Treger, Spintronics: A spin-based electronics vision for the future, Science **294**, 1488 (2001).

[11] J. D. Koralek, C. P. Weber, J. Orenstein, B. A. Bernevig, S.-C. Zhang, S. Mack, and D. D. Awschalom, Emergence of the persistent spin helix in semiconductor quantum wells, Nature (London) **458**, 610 (2009).

[12] J. Li *et al.*, Spin current from sub-terahertz-generated antiferromagnetic magnons, Nature (London) **578**, 70 (2020).

[13] I. Ilyakov, A. Brataas, T. V. A. G. de Oliveira, A. Ponomaryov, J.-C. Deinert, O. Hellwig, J. Faßbender, J. Lindner, R. Salikhov, and S. Kovalev, Efficient ultrafast field-driven spin current generation for spintronic terahertz frequency conversion, Nat. Commun. **14**, 7010 (2023).

[14] X. Yang *et al.*, Anisotropic nonlocal damping in ferromagnet/α–GeTe bilayers enabled by splitting energy bands, Phys. Rev. Lett. **131**, 186703 (2023).

[15] H. Zhang, C.-X. Liu, X.-L. Qi, X. Dai, Z. Fang, and S.-C. Zhang, Topological insulators in Bi_2Se_3, Bi_2Te_3 and Sb_2Te_3 with a single Dirac cone on the surface, Nat. Phys. **5**, 438 (2009).

[16] S. Basak, H. Lin, L. A. Wray, S. Y. Xu, L. Fu, M. Z. Hasan, and A. Bansil, Spin texture on the warped Dirac-cone surface states in topological insulators, Phys. Rev. B **84**, 121401(R) (2011).

[17] W. Jung *et al.*, Warping effects in the band and angular-momentum structures of the topological insulator Bi_2Te_3, Phys. Rev. B **84**, 245435 (2011).

[18] J. Sánchez-Barriga, M. R. Scholz, E. Golias, E. Rienks, D. Marchenko, A. Varykhalov, L. V. Yashina, and O. Rader, Anisotropic effect of warping on the lifetime broadening of topological surface states in angle-resolved photoemission from Bi_2Te_3, Phys. Rev. B **90**, 195413 (2014).

[19] L. Fu, Hexagonal warping effects in the surface states of the topological insulator Bi_2Te_3, Phys. Rev. Lett. **103**, 266801 (2009).

[20] P. He, S. S. L. Zhang, D. Zhu, Y. Liu, Y. Wang, J. Yu, G. Vignale, and H. Yang, Bilinear magnetoelectric resistance as a probe of three-dimensional spin texture in topological surface states, Nat. Phys. **14**, 495 (2018).

[21] P. B. Ndiaye, C. A. Akosa, M. H. Fischer, A. Vaezi, E. A. Kim, and A. Manchon, Dirac spin-orbit torques and charge pumping at the surface of topological insulators, Phys. Rev. B **96**, 014408 (2017).

[22] A. Brataas, Y. Tserkovnyak, G. E. W. Bauer, and P. J. Kelly, in *Spin Current* (Oxford University Press, New York, 2017).

[23] S. Yan, S. Tian, Y. Fu, F. Meng, Z. Li, H. Lei, S. Wang, and X. Zhang, Highly efficient room-temperature nonvolatile magnetic switching by current in Fe_3GaTe_2 thin flakes, Small **20**, e2311430 (2024).

[24] Y. Wang *et al.*, Room temperature magnetization switching in topological insulator-ferromagnet heterostructures by spin-orbit torques, Nat. Commun. **8**, 1364 (2017).

[25] L. Chen *et al.*, Emergence of anisotropic Gilbert damping in ultrathin Fe layers on GaAs(001), Nat. Phys. **14**, 490 (2018).

[26] A. A. Baker, A. I. Figueroa, C. J. Love, S. A. Cavill, T. Hesjedal, and G. van der Laan, Anisotropic absorption of pure spin currents, Phys. Rev. Lett. **116**, 047201 (2016).

[27] J. C. Slonczewski, Conductance and exchange coupling of two ferromagnets separated by a tunneling barrier, Phys. Rev. B **39**, 6995 (1989).

[28] R. Laiho and H. J. Reittu, Theory of scanning tunneling microscopy with spin-polarized electrons obtained from a semiconducting tip, Surf. Sci. **289**, 363 (1993).

[29] P. Schwab, R. Raimondi, and C. Gorini, Spin-charge locking and tunneling into a helical metal, Europhys. Lett. **93**, 67004 (2011).

[30] J.-n. Liu *et al.*, Surface coupling in Bi_2Se_3 ultrathin films by screened Coulomb interaction, Nat. Commun. **14**, 4424 (2023).

[31] Y. Y. Li *et al.*, Intrinsic topological insulator Bi_2Te_3 thin films on Si and their thickness limit, Adv. Mater. **22**, 4002 (2010).

[32] See Supplemental Material at http://link.aps.org/supplemental/10.1103/PhysRevLett.134.236204 for details of measurements, derivations and methods, which includes Refs. [33–38].

[33] B. Zhou, H. Z. Lu, R. L. Chu, S. Q. Shen, and Q. Niu, Finite size effects on helical edge states in a quantum spin-Hall system, Phys. Rev. Lett. **101**, 246807 (2008).

[34] Y. Zhang *et al.*, Crossover of the three-dimensional topological insulator Bi_2Se_3 to the two-dimensional limit, Nat. Phys. **6**, 584 (2010).

[35] T. Yokoyama and Y. Tserkovnyak, Spin diffusion and magnetoresistance in ferromagnet/topological-insulator junctions, Phys. Rev. B **89**, 035408 (2014).

[36] H.-P. Xue *et al.*, Synergistic enhancement of Gilbert damping and spin relaxation time in Fe/Bi_2Te_3 heterostructure, Phys. Rev. B **111**, 075104 (2025).

[37] R. Sun *et al.*, Visualizing tailored spin phenomena in a reduced-dimensional topological superlattice, Adv. Mater. **32**, 2005315 (2020).

[38] T. Valla, A. V. Fedorov, P. D. Johnson, and S. L. Hulbert, Many-body effects in angle-resolved photoemission: Quasiparticle energy and lifetime of a Mo(110) surface state, Phys. Rev. Lett. **83**, 2085 (1999).

[39] Y. T. Fanchiang, K. H. M. Chen, C. C. Tseng, C. C. Chen, C. K. Cheng, S. R. Yang, C. N. Wu, S. F. Lee, M. Hong, and J. Kwo, Strongly exchange-coupled and surface-state-modulated magnetization dynamics in Bi_2Se_3/ yttrium iron garnet heterostructures, Nat. Commun. **9**, 223 (2018).

[40] H. Tu *et al.*, Large anisotropy of magnetic damping in amorphous CoFeB films on GaAs(001), J. Phys. Condens. Matter **32**, 335804 (2020).

[41] T. Seifert *et al.*, Efficient metallic spintronic emitters of ultrabroadband terahertz radiation, Nat. Photonics **10**, 483 (2016).

[42] E. Beaurepaire, J. C. Merle, A. Daunois, and J. Y. Bigot, Ultrafast spin dynamics in ferromagnetic nickel, Phys. Rev. Lett. **76**, 4250 (1996).

[43] H. Park, S. Rho, J. Kim, H. Kim, D. Kim, C. Kang, and M.-H. Cho, Topological surface-dominated spintronic THz emission in topologically nontrivial $Bi_{1-x}Sb_x$ films, Adv. Sci. **9**, 2200948 (2022).

[44] E. Rongione *et al.*, Spin-momentum locking and ultrafast spin-charge conversion in ultrathin epitaxial $Bi_{1-x}Sb_x$ topological insulator, Adv. Sci. **10**, e2301124 (2023).

[45] M. Battiato, P. Maldonado, and P. M. Oppeneer, Treating the effect of interface reflections on superdiffusive spin transport in multilayer samples (invited), J. Appl. Phys. **115**, 172661 (2014).

[46] B. Koopmans, G. Malinowski, F. Dalla Longa, D. Steiauf, M. Fahnle, T. Roth, M. Cinchetti, and M. Aeschlimann, Explaining the paradoxical diversity of ultrafast laser-induced demagnetization, Nat. Mater. **9**, 259 (2010).

[47] B. Koopmans, J. J. Ruigrok, F. D. Longa, and W. J. de Jonge, Unifying ultrafast magnetization dynamics, Phys. Rev. Lett. **95**, 267207 (2005).